Available online at www.sciencedirect.com

ScienceDirect

Ceramics International 40 (2014) 3155–3163

CERAMICS INTERNATIONAL

www.elsevier.com/locate/ceramint

Conventional- and microwave-hydrothermal synthesis of $LiMn_2O_4$: Effect of synthesis on electrochemical energy storage performances

Kunfeng Chen[a,c], Ailaura C. Donahoe[b], Young Dong Noh[b], Keyan Li[c], Sridhar Komarneni[b,*], Dongfeng Xue[a,c,**]

[a]State Key Laboratory of Rare Earth Resource Utilization, Changchun Institute of Applied Chemistry, Chinese Academy of Sciences, Changchun 130022, PR China
[b]Materials Research Institute, Materials Research Laboratory, The Pennsylvania State University, University Park, PA 16802, USA
[c]School of Chemical Engineering, Dalian University of Technology, Dalian 116024, PR China

Received 8 September 2013; received in revised form 26 September 2013; accepted 27 September 2013
Available online 8 October 2013

Abstract

The $LiMn_2O_4$ electrode materials were synthesized by the conventional-hydrothermal and microwave-hydrothermal methods. The electrochemical performances of $LiMn_2O_4$ were studied as supercapacitors in $LiNO_3$ electrolyte and lithium-ion battery cathodes. The microwave-hydrothermal method can synthesize $LiMn_2O_4$ electrode materials with reversible electrochemical reaction in a short reaction time and low reaction temperature than conventional-hydrothermal route. The capacitance of $LiMn_2O_4$ electrode increased with increasing crystallization time in conventional-hydrothermal route. The results showed that $LiMn_2O_4$ supercapacitors had similar discharge capacity and potential window (1.2 V) as that of ordinary lithium-ion battery cathodes. In $LiNO_3$ aqueous electrolyte, the reaction kinetics of $LiMn_2O_4$ supercapacitors was very fast. Even, at current densities of 1 A/g and 5 A/g, aqueous electrolyte gave good capacity compared with that in organic electrolyte at a current density of 0.05 A/g.

Keywords: $LiMn_2O_4$; Supercapacitors; Lithium-ion battery; Cathode; $LiNO_3$ aqueous electrolyte

1. Introduction

The demand for electrical energy has significantly increased with the rapid growth of the global economy and population [1,2]. Lithium-ion batteries and supercapacitors are important energy storage systems, which have received much interest [3,4]. Aqueous rechargeable lithium battery, which uses aqueous electrolytes and lithium intercalation compounds as electrodes based on redox reaction, has led to a brand-new area of research of the lithium ion batteries in the mid-1990s [5,6] due to their low capital investment, high ion conductivity, reliability and good safety [7,8]. The aqueous rechargeable lithium ion battery is considered as environmentally benign compared with the organic electrolyte [9]. Much of the early work on aqueous rechargeable lithium battery involved the use of $LiMn_2O_4$ as the positive electrode [9,10]. However, the study of capacitance of $LiMn_2O_4$ supercapacitors in aqueous electrolyte and the lithium-ion battery cathode performances of $LiMn_2O_4$ electrodes were rarely studied. A systematic study of the electrochemical performance of electrode materials with different morphologies and structures may lead to better supercapacitors and batteries.

Here, we synthesized $LiMn_2O_4$ with conventional-hydrothermal (C-H) and microwave-hydrothermal (M-H) methods. Then, the electrochemical performances of $LiMn_2O_4$ supercapacitors in aqueous $LiNO_3$ electrolyte were firstly studied. The $LiMn_2O_4$ electrode materials were also assembled into conventional lithium-ion batteries and their electrochemical performances as cathodes were studied. The results showed that $LiMn_2O_4$ supercapacitors had similar discharge capacity and potential window (1.2 V) as that of ordinary lithium-ion battery. The electrochemical performance tests showed that the specific capacity of $LiMn_2O_4$ as the supercapacitor material is similar to that of ordinary lithium-ion battery with organic electrolyte. In aqueous electrolyte, the

*Correspondence to: 205, Materials Research Laboratory, The Pennsylvania State University, University Park, PA 16802, USA. Tel.: +1 814 865 1542; fax: +1 814 865 2326.
**Corresponding author.
E-mail addresses: Komarneni@psu.edu (S. Komarneni), dongfeng@ciac.ac.cn (D. Xue).

0272-8842/$ - see front matter © 2013 Elsevier Ltd and Techna Group S.r.l. All rights reserved.
http://dx.doi.org/10.1016/j.ceramint.2013.09.128

reaction kinetics of supercapacitors became very fast and gave good capacitance.

2. Experimental

2.1. Synthesis of $LiMn_2O_4$

In a typical synthesis of $LiMn_2O_4$, 5.6 mmol of $MnCl_2 \cdot 4H_2O$ and 2.4 mmol of $KMnO_4$ were dissolved in 20 ml of H_2O in a Teflon vessel. After that, 12 mmol of LiOH was dissolved in a 20 ml H_2O and this solution was added slowly to the above solution mixture under stirring. The final mixture was treated conventional-hydrothermally or microwave-hydrothermally at different temperatures and durations. The resultant reaction products were separated from solutions by centrifugation and were washed several times with deionized water and ethanol followed by drying.

2.2. Synthesis of lithium manganese nickel oxide: $LiMn_{1.53}Ni_{0.47}O_{3.67}$ (grinding)

For this synthesis, 3.1868 g of $Mn(CH_3COO)_2 \cdot 4H_2O$, 2.0356 g of $Ni(NO_3)_2 \cdot 6H_2O$, and 1.8462 g of $LiNO_3$ were ground and mixed thoroughly using a mortar and a pestle. After mixing, the mixture was transferred to a Pt-crucible and heated in a conventional furnace at 450 °C for 4 h. The resultant reaction product was washed several times with deionized water and ethanol.

2.3. Synthesis of lithium manganese nickel oxide: $LiMn_{1.53}Ni_{0.47}O_{3.67}$ (mixing in a crucible)

For this, 2.7940 g of $Mn(CH_3COO)_2 \cdot 4H_2O$, 1.8612 g of $Ni(NO_3)_2 \cdot 6H_2O$, and 1.5305 g of $LiNO_3$ were mixed thoroughly in a Pt-crucible using a spatula. However, no grinding was used in this case. After mixing, the mixture was heated in a furnace at 450 °C and 750 °C for 4 h. The resultant reaction products were washed several times with deionized water and ethanol as above followed by drying.

2.4. Characterization

The prepared samples were characterized by powder X-ray diffraction (XRD) for phase detection. Powder XRD patterns were obtained on a PANalytical X'Pert MPD diffractometer operated at 45 kV voltage and 40 mA current with a PIXcel detector and using Cu Kα radiation. Field-emission scanning electron microscope (FESEM, Hitachi-S4800) was used to determine the particle size and shape of synthesized materials.

2.5. Testing as supercapacitors

Working electrodes were prepared by pressing a mixture of each sample, acetylene black, and polyvinylidene fluoride (PVDF) in a weight ratio of 80:10:10 on porous nickel foil. All experiments were performed in a three-electrode open beaker cell in 1 M $LiNO_3$ under normal atmosphere. The $LiMn_2O_4$/nickel foam was used as the working electrode, saturated calomel electrode (SCE) as the reference electrode, and the Pt wire as a counter electrode. The cyclic voltammetry (CV), and galvanostatic charge–discharge measurements were carried out by an electrochemical workstation (CHI 660D).

2.6. Testing as lithium-ion batteries

The working electrodes were prepared by mixing each active material, acetylene black, and polyvinylidene fluoride (PVDF) in a weight ratio of 80:10:10. The mixtures were treated with N-methyl-2-pyrrolidone, and pasted onto aluminum foil as cathodes. For the electrochemical properties, coin cells (CR2025) were fabricated using lithium metal as the counter electrode. 1 M $LiPF_6$ in ethylene carbonate/dimethyl carbonate/diethyl carbonate (EC/DMC/DEC, 1:1:1 vol%) served as the electrolyte. A galvanostatic cycling test of the assembled half-cells was conducted on a LAND CT2001A system.

3. Results and discussion

The $LiMn_2O_4$ electrode materials were synthesized by the conventional-hydrothermal (C-H) and microwave-hydrothermal (M-H) methods. The only phase present in the reaction products was $LiMn_2O_4$ as can be seen in XRD patterns of both C-H synthesis (Fig. 1) and M-H synthesis (Fig. 2). XRD proved that pure $LiMn_2O_4$ was crystallized at 150–200 °C with treatment times of 1–18 h under both C-H and M-H conditions (Table 1). Fig. 1 shows the crystallization of $LiMn_2O_4$ as a function of time at 200 °C. Highly crystalline $LiMn_2O_4$ was obtained after 2, 3 and 18 h of treatment time but slightly less crystalline material was obtained after 1 h of treatment time (Fig. 1a). It appears that at least 2 h of treatment time was necessary at 200 °C to get a highly crystalline $LiMn_2O_4$ under C-H conditions. However, $LiMn_2O_4$ was crystallized at both 150 and 165 °C within 1 h under M-H conditions. The XRD patterns of $LiMn_2O_4$ prepared under M-H and C-H conditions at 150 °C for different treatment times are

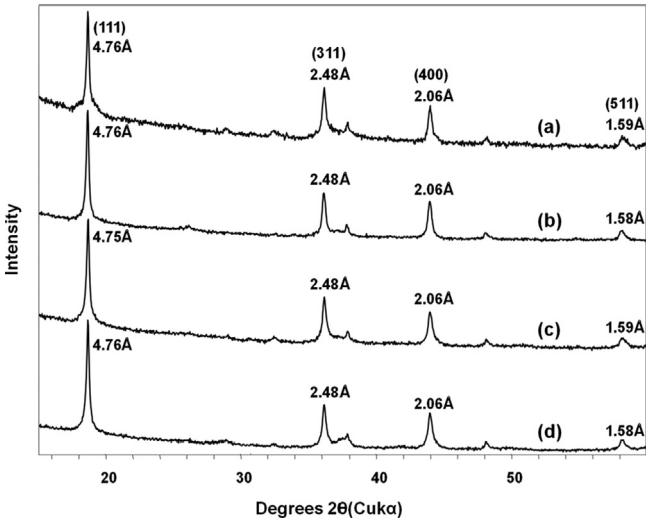

Fig. 1. XRD patterns of $LiMn_2O_4$ prepared at 200 °C under conventional-hydrothermal conditions for 1 h (a), 2 h (b), 3 h (c), and 18 h (d).

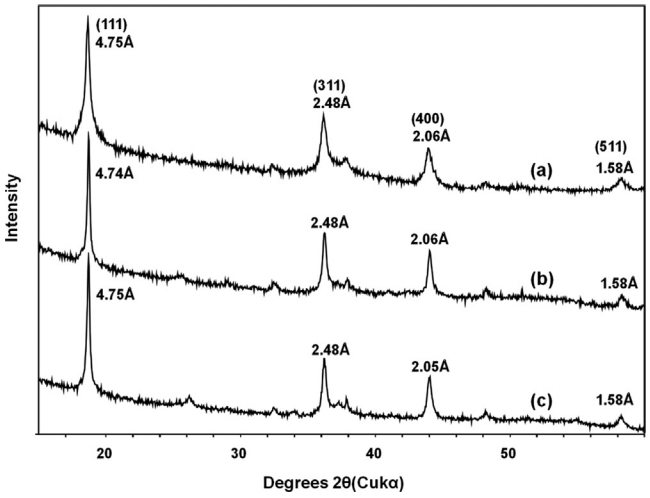

Fig. 2. XRD patterns of $LiMn_2O_4$ prepared under microwave-hydrothermal conditions at 150 °C for 1 h (a) and conventional-hydrothermal conditions at 150 °C (b) for 3 h and (c) for 18 h.

Table 1
Phase, synthesis conditions and specific capacitances in 1 M $LiNO_3$ aqueous electrolyte of the as-obtained products.

Sample no.	Phase	Synthesis conditions	Specific capacitance F/g (1.2 V)	
			1 A/g	5 A/g
1	$LiMn_2O_4$	CH 200 °C 1 h	163	100
2	$LiMn_2O_4$	CH 200 °C 2 h	167	108
3	$LiMn_2O_4$	CH 200 °C 3 h	206	125
4	$LiMn_2O_4$	CH 200 °C 18 h	237	160
5	$LiMn_2O_4$	CH 170 °C 3 h	192	109
6	$LiMn_2O_4$	CH 170 °C 18 h	213	151
7	$LiMn_2O_4$	CH 150 °C 3 h	181	109
8	$LiMn_2O_4$	CH 150 °C 18 h	203	130
9	$LiMn_2O_4$	MH 150 °C 1 h	230	144
10	$LiMn_2O_4$	MH 165 °C 1 h	271	211
11	$Li[Mn_{1.53}Ni_{0.47}O_{3.67}]$	450 °C 4 h grinding	80	–
12	$Li[Mn_{1.53}Ni_{0.47}O_{3.67}]$	450 °C 4 h mixing	33	–
13	$Li[Mn_{1.53}Ni_{0.47}O_{3.67}]$	700 °C 4 h mixing	23	–

CH = conventional-hydrothermal.
MH = microwave-hydrothermal.

compared in Fig. 2. Although the main peak of $LiMn_2O_4$ prepared under M-H condition at 150 °C for 1 h appears broader than those prepared by the C-H method for 3 (Fig. 2b) or 18 h (Fig. 2b), it is very crystalline (Fig. 2a) and similar to the peak of $LiMn_2O_4$ prepared under C-H conditions at 200 °C/1 h (Fig. 1a). M-H process led to a similar $LiMn_2O_4$ at 150 °C/1 h (Fig. 2a) as that of 200 °C/1 h under C-H conditions (Fig. 1a) suggesting that synthesis occurs at lower temperatures by the M-H method as has been shown before for many other materials by us [4,11–13]. Fig. 3 shows the formation of highly crystalline $Li[Mn_{1.53}Ni_{0.47}O_{3.67}]$ either by grinding and heating at 450 °C/4 h (Fig. 3a) or simple mixing and heating at 450 °C/4 h (Fig. 3b) or simple mixing and heating at 700 °C/4 h (Fig. 3c) using conventional furnace heating. These materials are compared with the $LiMn_2O_4$ materials prepared under both C-H and M-H conditions.

Fig. 4 shows the SEM images of $LiMn_2O_4$ synthesized at different temperatures and reaction times with the C-H methods. With the reaction time extending to 18 h at 200 °C, the morphology of $LiMn_2O_4$ materials changed from block-like to piece-like and finally to rod-like morphologies (Fig. 4). The spinel $LiMn_2O_4$ has a cubic structure with the space group of Fd3m symmetry, in which Li and Mn ions occupy tetrahedral (8a) sites and octahedral (16d) sites, respectively, within a cubic close-packed oxygen array with oxygen ions in 32e sites. Therefore, the single crystalline 1-D $LiMn_2O_4$ cannot be easily obtained. The 1-D $LiMn_2O_4$ nanostructures can be obtained by the use of 1-D MnO_2 nanostructures as a self-template. In our synthesis system, 1-D MnO_2 nanostructures can be easily synthesized [4]. With the presence of LiOH, the MnO_2 nanorods can convert into $LiMn_2O_4$ rods by chemical transformation.

At 150 and 170 °C similar morphologies were observed as those observed at 200 °C (Fig. 4). It is interesting to note that the reaction temperature and time in M-H routes are lower than those of C-H routes (Table 1). The enhanced reaction rates at lower temperatures can be ascribed to localized superheating during the microwave-hydrothermal process [14]. The coupled microwave and hydrothermal method possesses advantages of both hydrothermal and microwave conditions, which can accelerate the reaction rate while keeping the same morphology and phase [4,11–13]. Fig. 5 shows the morphologies of $LiMn_2O_4$ synthesized by the M-H method for comparison with those of C-H method. Mainly block-like shapes were obtained at low reaction temperature of 150 °C/1 h but piece-like and rod-like $LiMn_2O_4$ was formed at a slightly higher temperature of 165 °C/1 h. The morphologies of lithium manganese nickel oxides prepared at 450 °C and 700 °C under conventional furnace heating are shown in Fig. 6. At 450 °C, poor definition of individual crystals (Fig. 6a) and some aggregation (Fig. 6b) could be seen while

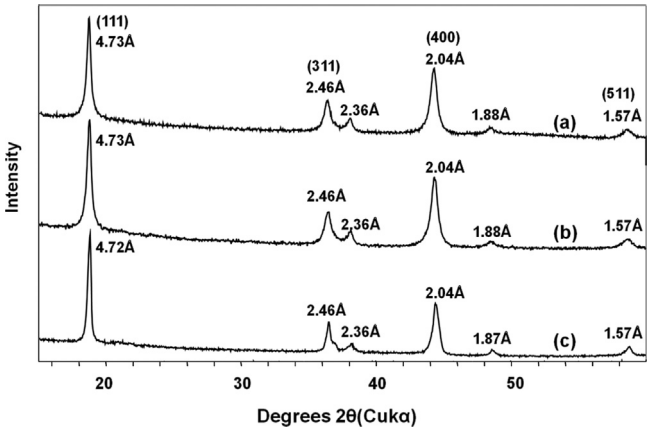

Fig. 3. XRD patterns of $LiMn_{1.53}Ni_{0.47}O_{3.67}$ prepared for 4 h: grinding and heating at 450 °C (a), mixing and heating at 450 °C (b), and mixing and heating at 700 °C (c).

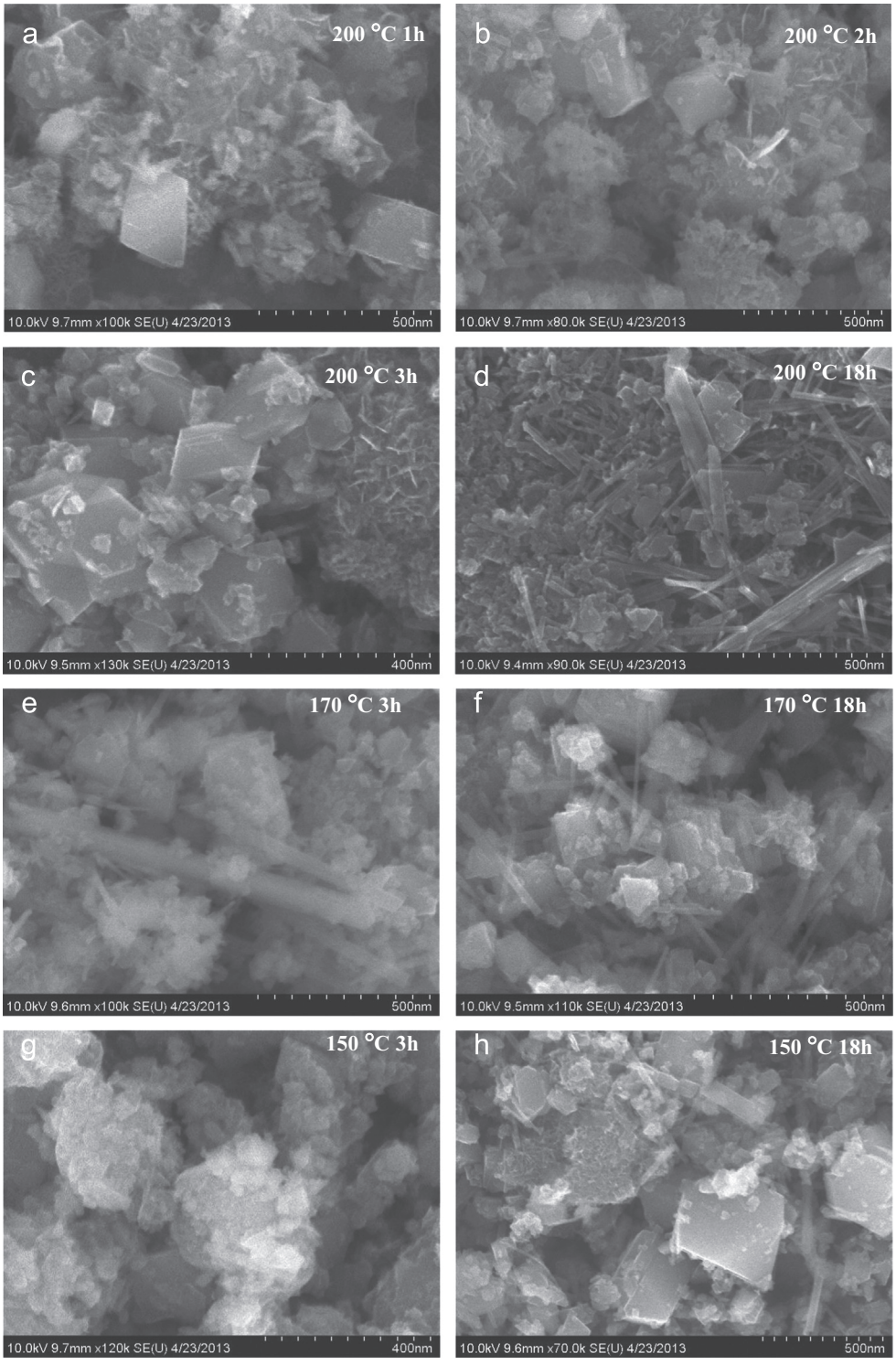

Fig. 4. SEM images of $LiMn_2O_4$ synthesized by the conventional-hydrothermal methods at different reaction temperatures and times.

well-defined crystals were obtained at a higher temperature of 700 °C (Fig. 6c).

The electrochemical performances of $LiMn_2O_4$ were firstly evaluated as supercapacitors in 1M $LiNO_3$. The CV curves of $LiMn_2O_4$ obtained with conventional-hydrothermal route at the scan rate of 10 mV/s are shown in Fig. 7. There are two redox couples situated at 0.89/0.55 V and 1.05/0.75 V (vs. SCE). These redox peaks correspond to the de-intercalation and intercalation of Li^+ ions from/into the spinel host structure in the aqueous electrolyte [7,10]. The theoretical stable window of water is 1.229 V. The measured potential window is from 0 to 1.2 V without oxygen and hydrogen evolution,

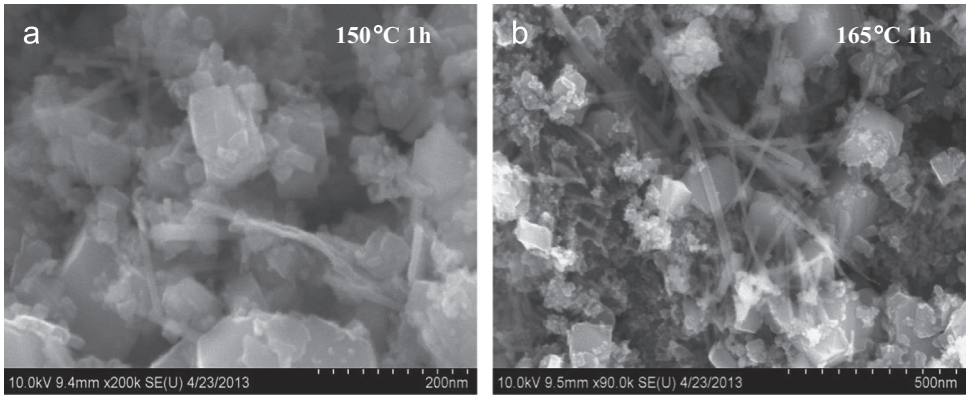

Fig. 5. SEM images of $LiMn_2O_4$ synthesized by microwave-hydrothermal route at 150 °C/1 h (a) and 165 °C/1 h (b).

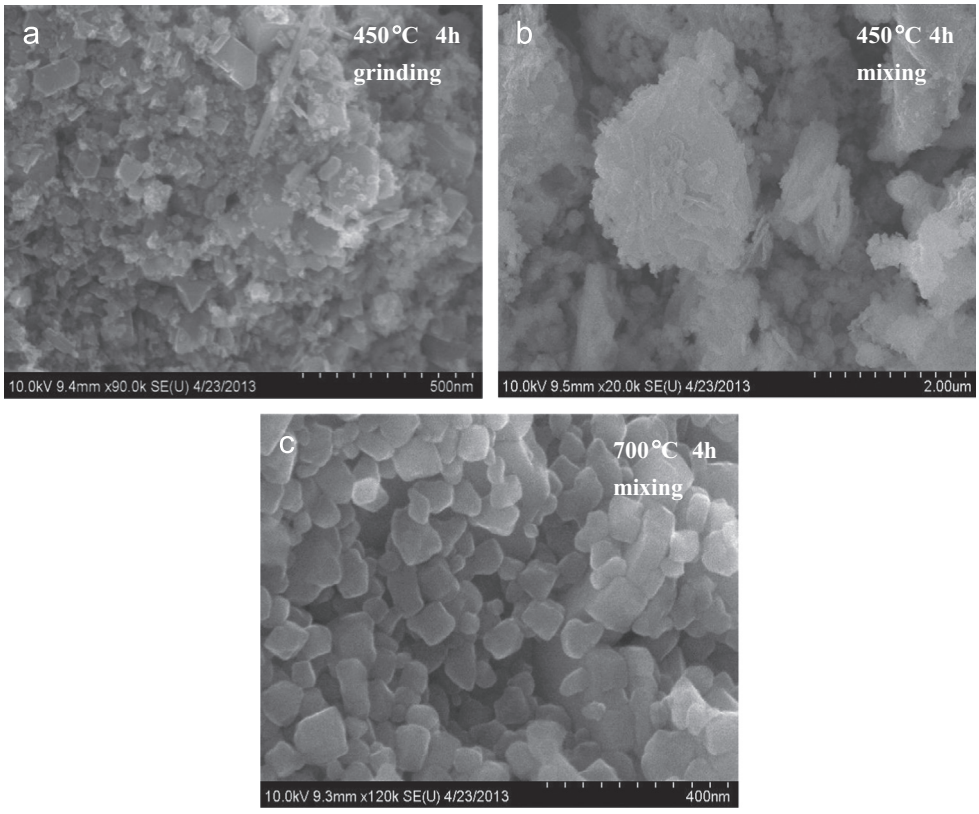

Fig. 6. SEM images of $LiMn_{1.53}Ni_{0.47}O_{3.67}$ sample synthesized by conventional furnace heating in air: (a) 450 °C 4 h-grinding (b) 450 °C 4 h-mixing and (c) 700 °C 4 h-mixing.

which indicated that $LiMn_2O_4$ is very stable for the reversible de-intercalation/intercalation reaction in the aqueous electrolyte. The redox reactions of $LiMn_2O_4$ are as follows:

$$LiMn_2O_4 \leftrightarrow Li_{1-x}Mn_2O_4 + xLi^+ + xe^- \quad (1)$$

Li^+ cations de-intercalate from the tetrahedral 8a- and octahedral 16c-sites and lead to two redox couples [7]. The $LiMn_2O_4$ obtained at different reaction times show similar CV curves with two redox peaks. When the scan rate was increased to 50 mV/s, the currents were increased and the shapes of CV curves were changed without any evidence for the presence of two redox couples.

Figs. 7a2–d2 show the galvanostatic charge–discharge curves of $LiMn_2O_4$ at different current densities in 1 M $LiNO_3$ electrolyte. Two sloping voltage ranges in charge (or discharge) curves correspond to two redox couples in CV curves. The value of the specific capacitance was obtained from the charge–discharge cycling measurements according to the following equation [15]:

$$C = \frac{I\,\Delta t}{m\,\Delta V} \quad (2)$$

where I is the current used for charge/discharge in A, Δt is the time elapsed for the discharge cycle in s, m is the mass of the

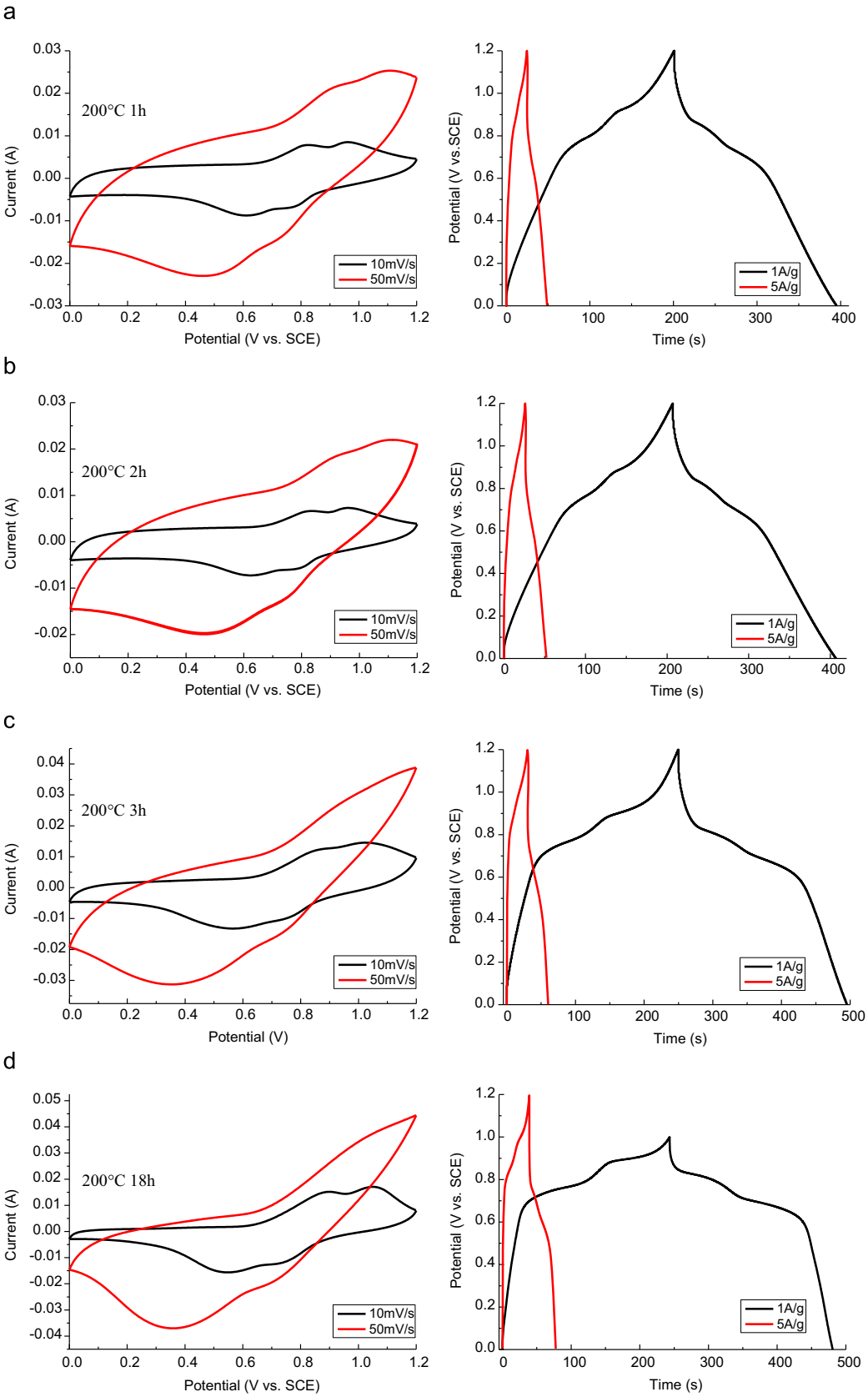

Fig. 7. CV curves and galvanostatic charge–discharge curves of $LiMn_2O_4$ synthesized by conventional-hydrothermal route at 200 °C for different reaction times in 1 M $LiNO_3$ electrolyte.

active electrode material in g, and ΔV is the voltage interval of the charge or discharge in V. The obtained capacities of different $LiMn_2O_4$ aqueous electrodes are shown in Table 1. The capacity of $LiMn_2O_4$ electrode increased with the prolonged crystallization time (Table 1) showing a correlation with crystallinity. When the current density was increased to 5 A/g, the capacity decreased (Table 1). When the hydrothermal crystallization time was longer, well-crystallized $LiMn_2O_4$ was obtained, which showed reversible de-intercalation/intercalation reaction.

The electrochemical performances of samples synthesized using microwave-hydrothermal routes were also evaluated as supercapacitors in 1 M $LiNO_3$. Fig. 8 shows CV curves and galvanostatic charge–discharge curves of $LiMnO_4$ synthesized by M-H route at different reaction temperatures for 1 h. The CV and galvanostatic charge–discharge curves of $LiMn_2O_4$ obtained at both 150 °C and 165 °C temperatures show two redox couples and their capacity can reach >230 F/g. The M-H route is amenable to synthesize $LiMn_2O_4$ electrode materials with reversible electrochemical reaction and better capacitance (Table 1) in a short reaction time and low reaction temperature than by the C-H routes.

In order to evaluate the electrochemical performance of a $LiMn_2O_4$, we also assembled coin cells using lithium metal as the counter electrode and 1 M $LiPF_6$ in ethylene carbonate/dimethyl carbonate/diethyl carbonate (EC/DMC/DEC, 1:1:1 vol%) as the electrolyte [16,17]. The galvanostatic charge–discharge curves of $LiMn_2O_4$ are shown in Fig. 9. Two sloping voltage ranges in charge (or discharge) curves are also present, which corresponds to two redox couples in CV curves (reaction (1)), similar to the behavior in aqueous $LiNO_3$ electrolytes. The potential window is 1.3 V (from 3.0 to 4.3 V vs. Li^+/Li), which is comparable with the potential window of 1.2 V of aqueous $LiNO_3$ electrolyte. The cycling performances of $LiMn_2O_4$ can also be found in Fig. 9 and Table 2. It should be pointed out that the reaction kinetics became very fast in aqueous $LiNO_3$ electrolyte. The current density in $LiNO_3$ electrolyte reached 5 A/g, while the current density in organic electrolyte was 0.05 A/g.

During electrochemical reaction process, $LiMn_2O_4$ often undergoes the phase transition from cubic to tetragonal phase, often referred to as Jahn–Teller distortion, which is accompanied by a 6.5% increase in the unit cell volume [10]. Therefore, the structural integrity of the electrode was damaged during charge/discharge cycling that result in rapid capacity fading. The cationic substitutions have been developed to overcome the detrimental effects. $LiMn_{1.53}Ni_{0.47}O_{3.67}$ was synthesized to evaluate the role of cationic substitutions on electrochemical performances. Table 1 shows the specific capacitance of $LiMn_{1.53}Ni_{0.47}O_{3.67}$ in $LiNO_3$ electrolyte. The specific capacitances of $LiMn_{1.53}Ni_{0.47}O_{3.67}$ are no more than 80 F/g, which are much lower than that of $LiMn_2O_4$ (>160 F/g). In essence, Ni can cause decrease in capacitance due to its larger atom weight than that of Mn. Especially, the Ni and

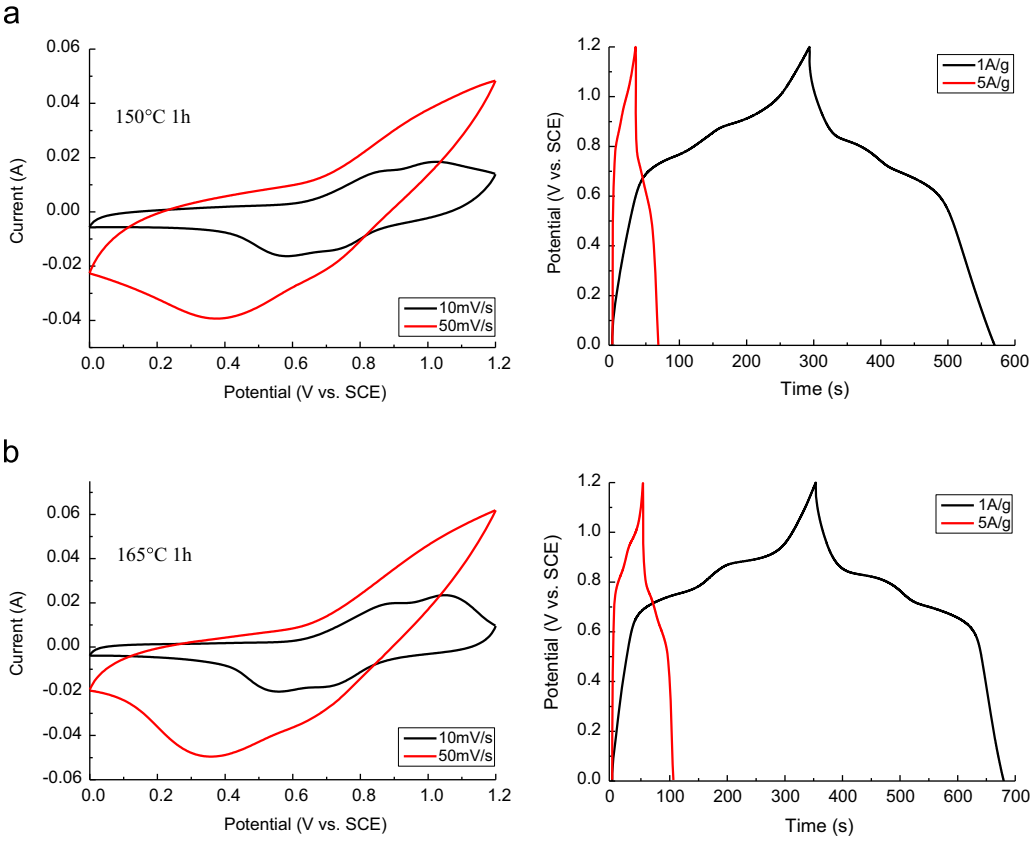

Fig. 8. CV curves and galvanostatic charge–discharge curves of $LiMn_2O_4$ synthesized by microwave-hydrothermal routes at different reaction temperatures and times in 1 M $LiNO_3$ electrolyte.

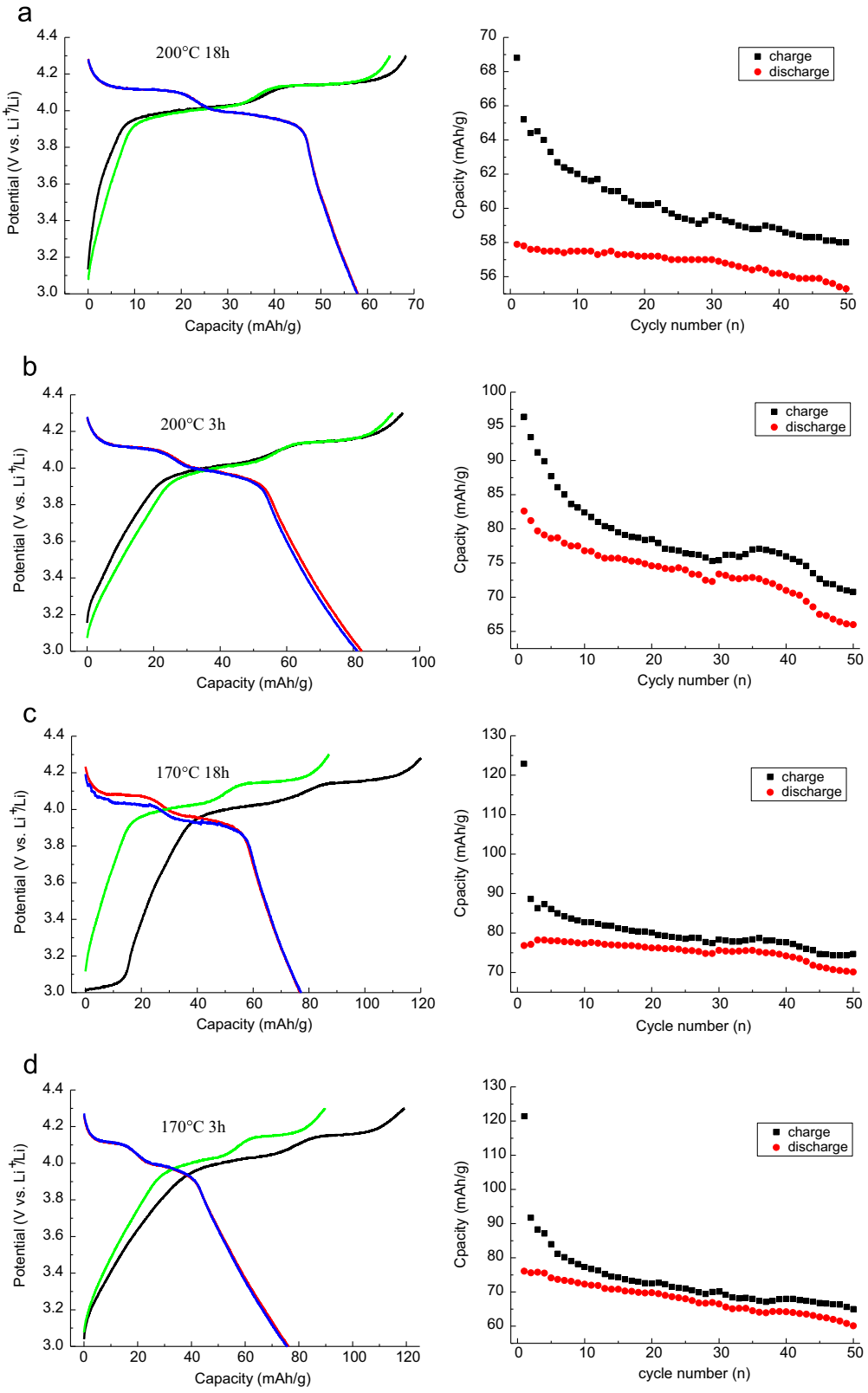

Fig. 9. Galvanostatic charge–discharge curves and cycling performances of $LiMn_2O_4$ cathodes synthesized by conventional-hydrothermal route at different reaction temperatures and times in organic electrolyte.

Mn cations have different electrochemical stable potential windows in aqueous electrolyte. In the potential window of 0–1.2 V, the Ni cation in $LiMn_{1.53}Ni_{0.47}O_{3.67}$ is not stable, which destroys the electrode structure and reduces the specific capacitance. As lithium-ion battery cathodes in organic electrolyte, the difference in capacity of $LiMn_{1.53}Ni_{0.47}O_{3.67}$ and $LiMn_2O_4$ is small (Table 2), which further proves our explanation.

Table 2
Capacities of the as-obtained products when used as lithium-ion battery cathodes in organic electrolyte.

Sample no.	Cathode capacity, mAh/g				
	1st	2nd	10th	20th	30th
1	70.3	70.2	60.5	56.3	53.2
2	65.8	63.8	55.8	51.2	48.9
3	82.6	81.2	76.8	74.6	73.4
4	57.9	57.8	57.5	57.2	57
5	76.1	75.6	72.3	69.8	66.5
6	76.8	77.1	77.3	76.2	75.6
7	71.3	68.8	63.6	59	56.7
8	78	78.3	78.5	73.3	71.1
9	69.4	70.2	67.6	61.3	62
10	61.9	74.5	74.2	72.4	73
11	83.2	79.9	65.7	53.8	47.4
12	71.5	69.3	61.2	50.3	43.7
13	54.1	50	45.5	41.6	41.1

4. Summary

In summary, $LiMn_2O_4$ materials were synthesized by conventional-hydrothermal and microwave-hydrothermal methods. The electrochemical performances of $LiMn_2O_4$ materials as supercapacitors in aqueous $LiNO_3$ electrolyte and lithium-ion battery cathodes in organic electrolyte were studied. The microwave-hydrothermal method can synthesize $LiMn_2O_4$ electrode materials with reversible electrochemical reaction in a short reaction time and low reaction temperature than conventional-hydrothermal route. The specific capacitance of $LiMn_2O_4$ electrode increased with increasing crystallization time in conventional-hydrothermal route. The results showed that $LiMn_2O_4$ supercapacitors had similar discharge capacity and potential window (1.2 V) as that of ordinary lithium-ion battery cathodes. In aqueous electrolyte, the reaction kinetics was very fast. At current densities of 1 A/g and 5 A/g, the supercapacitors gave good specific capacitance in 1 M $LiNO_3$ aqueous electrolyte.

Acknowledgment

Financial support from the National Natural Science Foundation of China (Grant nos. 50872016, 20973033 and 51125009), the National Natural Science Foundation for Creative Research Group (Grant no. 21221061) and the Hundred Talents Program of the Chinese Academy of Sciences is acknowledged.

References

[1] B. Dunn, H. Kamath, J.M. Tarascon, Electrical energy storage for the grid: a battery of choices, Science 334 (2011) 928.
[2] F. Liu, S. Song, D. Xue, H. Zhang, Folded structured graphene paper for high performance electrode materials, Advanced Materials 24 (2012) 1089.
[3] J. Liu, H. Xia, D. Xue, L. Lu, Double-shelled nanocapsules of V_2O_5-based composites as high-performance anode and cathode materials for Li ion batteries, Journal of the American Chemical Society 131 (2009) 12086.
[4] K. Chen, Y.D. Noh, K. Li, S. Komarneni, D. Xue, Microwave-hydrothermal crystallization of polymorphic MnO_2 for electrochemical energy storage, Journal of Physical Chemistry C 117 (2013) 10770.
[5] L. Wu, J.R. Dahn, D.S. Wainwright, Rechargeable lithium batteries with aqueous electrolytes, Science 264 (1994) 1115.
[6] Y. Lu, J.B. Goodenough, Y. Kim, Aqueous cathode for next-generation alkali-ion batteries, Journal of the American Chemical Society 133 (2011) 5756.
[7] X. Wang, Y. Hou, Y Zhu, Y. Wu, R. Holze, An aqueous rechargeable lithium battery using coated Li metal as anode, Scientific Reports 3 (2013) 1401.
[8] R. Ruffo, F. La Mantia, C. Wessells, R.A. Huggins, Y. Cui, Electrochemical characterization of $LiCoO_2$ as rechargeable electrode in aqueous $LiNO_3$ electrolyte, Solid State Ionics 192 (2011) 289.
[9] M. Zhao, Q. Zheng, F. Wang, W. Dai, X. Song, Electrochemical performance of high specific capacity of lithium-ion cell LiV_3O_8/$LiMn_2O_4$ with $LiNO_3$ aqueous solution electrolyte, Electrochimica Acta 56 (2011) 3781.
[10] W. Tang, S. Tian, L. Liu, L. Li, H.P. Zhang, Y.B. Yue, Y. Bai, Y.P. Wu, K. Zhu, Nanochain $LiMn_2O_4$ as ultra-fast cathode material for aqueous rechargeable lithium batteries, Electrochemistry Communications 13 (2011) 205.
[11] K. Chen, Y.D. Noh, S. Lin, S. Komarneni, D. Xue, Crystallization of MnO_2 by microwave-hydrothermal synthesis and its applications for supercapacitors and lithium-ion batteries, Materials Focus 2 (2013) 86.
[12] S. Komarneni, R. Roy, Titania gel spheres by a new sol–gel process, Materials Letters 3 (1985) 165.
[13] S. Komarneni, R. Roy, Q.H. Li, Microwave-hydrothermal synthesis of ceramic powders, Materials Research Bulletin 27 (1992) 1393.
[14] S. Komarneni, V.C. Menon, Q.H. Li, R. Roy, F.W. Ainger, Microwave-hydrothermal processing of $BiFeO_3$ and $CsAl_2PO_6$, Journal of the American Ceramic Society 79 (1996) 1409.
[15] Y. Zhang, C. Sun, P. Lu, K. Li, S. Song, D. Xue, Crystallization design of MnO_2 towards better supercapacitance, CrystEngComm 14 (2012) 5892.
[16] K. Chen, S. Song, D. Xue, Vapor-phase crystallization route to oxidized Cu foils in air as anode materials for lithium-ion batteries, CrystEngComm 15 (2013) 144.
[17] K. Chen, D. Xue, Chemoaffinity-mediated crystallization of Cu_2O: a reaction effect on crystal growth and anode property, CrystEngComm 15 (2013) 1739.